Flamite, (Ca,Na,K)$_2$(Si,P)O$_4$, a new mineral from ultrahigh-temperature combustion metamorphic rocks, Hatrurim Basin, Negev Desert, Israel

E. V. Sokol[1], Y. V. Seryotkin[1,2], S. N. Kokh[1,*], Ye. Vapnik[3], E. N. Nigmatulina[1], S. V. Goryainov[1], E. V. Belogub[4] AND V. V. Sharygin[1,2]

[1] V.S. Sobolev Institute of Geology and Mineralogy, Siberian Branch of Russian Academy of Sciences, 3 Koptug Avenue, Novosibirsk, 630090, Russia
[2] Novosibirsk State University, 2 Pirogov Street, Novosibirsk, 630090, Russia
[3] Department of Geological and Environmental Sciences, Ben-Gurion University of the Negev, POB 653, Beer-Sheva 84105, Israel
[4] Institute of Mineralogy UrB RAS, Miass, 456317, Russia

ABSTRACT

Flamite (Ca,Na,K)$_2$(Si,P)O$_4$ ($P6_3$; a = 43.3726(18), c = 6.8270(4) Å; V = 11122.2(9) Å^3), a natural analogue of the P,Na,K-doped high-temperature α-Ca$_2$SiO$_4$ modification, is a new mineral from Ca- and Al-rich paralava, an ultrahigh-temperature combustion metamorphic melt rock. The type locality is situated in the southern Hatrurim Basin, the Negev Desert, Israel. Flamite occurs as regular lamellar intergrowths with partially hydrated larnite, together with rock-forming gehlenite, rankinite and Ti-rich andradite, minor ferrian perovskite, magnesioferrite, hematite, and retrograde ettringite and calcium silicate hydrates. The mineral is greyish to yellowish, transparent with a vitreous lustre, non-fluorescent under ultraviolet light and shows no parting or cleavage; Mohs hardness is 5−5½; calculated density is 3.264 g cm^{-3}. The empirical formula of holotype flamite (mean of 21 analyses) is (Ca$_{1.82}$Na$_{0.09}$K$_{0.06}$(Mg,Fe,Sr,Ba)$_{0.02}$)$_{\Sigma1.99}$(Si$_{0.82}$P$_{0.18}$)$_{\Sigma1.00}$O$_4$. The strongest lines in the powder X-ray diffraction pattern are [d, Å (I_{obs})]: 2.713(100), 2.765(44), 2.759(42), 1.762(32), 2.518(29), 2.402(23), 2.897(19), 1.967(18), 2.220(15), 1.813(15). The strongest bands in the Raman spectrum are 170, 260, 520, 538, 850, 863, 885, 952 and 1003 cm^{-1}.

KEYWORDS: flamite, new mineral, (Ca,Na,K)$_2$(Si,P)O$_4$, dicalcium silicate, α-Ca$_2$SiO$_4$, larnite, combustion metamorphism, Hatrurim Basin.

Introduction

THE new mineral flamite (Ca,Na,K)$_2$(Si,P)O$_4$ ($P6_3$; a = 43.3726(18), c = 6.8270(4) Å; V = 11122.2(9) Å^3) (IMA 2013-122) was discovered as a rock-forming mineral in Ca- and Al-rich paralava, an ultrahigh-temperature combustion metamorphic rock found in the Negev Desert, Israel. The type locality is situated in the Hatrurim

Basin and belongs to the largest complex of the unique Hatrurim Formation (Mottled Zone, MZ) in Israel (Bentor and Vroman, 1960; Gross, 1977; Burg *et al.*, 1992; Sokol *et al.*, 2008). Since the 1960s, numerous rare and new minerals, uncommon to natural systems, have been found in the MZ rocks. Most of them are natural analogues of phases found in industrial cement clinkers and/or concretes. The Hatrurim Basin is the type locality for bayerite, bentorite, ye'elimite, grossite, hatrurite, nagelschmidtite (Gross and Heller, 1963; Gross, 1977; 1980; 1984; Weber and Bischoff, 1994) and the recently

found barioferrite (Murashko *et al.*, 2011), shulamitite (Sharygin *et al.*, 2013), murashkoite (IMA 2012-071, Britvin *et al.*, 2013), zadovite (IMA 2013-031, Galuskin *et al.*, 2013*c*), gurimite (IMA 2013-032, Galuskina *et al.*, 2013), fluor-kyuygenite (IMA 2013-043, Galuskin *et al.*, 2013*b*), aradite (IMA 2013-047, Galuskin *et al.*, 2013*a*), negevite (IMA 2013-104, Britvin *et al.*, 2014*a*), halamishite (IMA 2013-105, Britvin *et al.*, 2014*b*), zuktamrurite (IMA 2013-107, Britvin *et al.*, 2014*c*), silicocarnotite (IMA 2013-139, Galuskin *et al.*, 2014).

The new mineral and mineral name have been approved by the International Mineralogical Association Commission on New Minerals, Nomenclature and Classification (IMA 2013-122). The name is derived from 'flame' and refers to the origin of the mineral by ultrahigh-temperature combustion metamorphism triggered by fossil-fuel ignition. The holotype specimen of flamite is stored in the collections of the Central Siberian Geological Museum of the V.S. Sobolev Institute of Geology and Mineralogy, Novosibirsk, Russia, catalogue number XIII-341/1.

Occurrence and association of flamite

Flamite occurs as a rock-forming mineral in a coarse-grained Ca-Al-rich paralava (holotype sample YV-402) (Fig. 1), an ultrahigh-temperature combustion metamorphic rock. The type locality is situated in the southern Hatrurim Basin (31º10′26′′N 35º17′31′′E), the Negev Desert, Israel. Within the Hatrurim Basin, there are numerous foci of high-temperature combustion metamorphism (represented by spurrite marble, larnite rocks, larnite-gehlenite, gehlenite and diopside-anorthite hornfelses), which coexist locally with ultrahigh-temperature melt rocks (paralavas) (Sharygin *et al.*, 2006; Vapnik *et al.*, 2007; Sokol *et al.*, 2008; Galuskin *et al.*, 2013*a*). Gehlenite hornfels with sporadic veins of gehlenite-bearing paralavas are distributed widely in the southern part of the Hatrurim Basin. Sample YV-402 is a thin paralava veinlet in gehlenite hornfels, which has experienced only slight retrograde alteration. It has a high CaO/SiO_2 ratio of 1.34 and contains (in wt.%) 30.89 SiO_2, 0.83 TiO_2, 11.00 Al_2O_3, 5.77 Fe_2O_3, 0.72 FeO, 0.02 MnO, 1.16 MgO, 41.44 CaO, 0.68 Na_2O, 0.42 K_2O and 2.45 P_2O_5, 0.94 H_2O, 0.97 CO_2. The mineral assemblage consists of ~40% Ca_2SiO_4 solid solutions (ss) (flamite as a regular lamellar intergrowth with partially hydrated larnite), ~30% gehlenite, 15% rankinite and 10% Ti-rich andradite (vol.%). Minor phases (~5 vol.%) are Fe-rich perovskite, magnesioferrite and hematite. Ti-rich andradite, gehlenite and occasionally rankinite, which contains tubular inclusions of cloudy flamite. Ettringite and calcium silicate hydrates are minor retrograde phases. The compositions of the rock-forming minerals are presented in Table 1.

Analytical methods

The flamite-bearing paralava was studied by optical thin section petrography, scanning electron-microscopy (SEM) and/or powder X-ray diffraction (PXRD) for quantification of the main constituents. *In situ* mineral chemistry was determined by electron microprobe (EMPA) at the V.S. Sobolev Institute of Geology and Mineralogy (IGM) in Novosibirsk. The bulk compositions of major elements were analysed by inductively coupled plasma atomic emission spectrometry (ICP-AES) at IGM. The optical properties of flamite were determined at the Institute of Mineralogy UrB RAS in Miass.

Microfabric and phase distribution were examined by LEO 420 SEM and JEOL JSM6380LA scanning electron microscopes on Au- and C-coated polished thin sections, at chamber vacuum pressures of 10^{-5} Torr (~0.01 Pa). Both instruments were operated at 10 kV and 2.0 nA beam current (measured in a Faraday cup).

The *in situ* chemical compositions of individual minerals were analysed by a JEOL JXA-8100 microprobe, in C-coated polished thin sections, with the chamber vacuum kept at 10^{-6} Torr (~0.001 Pa) or greater. The instrument was equipped with a single EDS spectrometer and five WDS spectrometers with LiF, PET or TAP crystals. Mineral chemistry was analysed at 20 kV and 15−30 nA, with 10 s counting time and a beam diameter of 2−3 μm. The compositions were estimated with reference to the natural and synthetic standards: wollastonite (Si, Ca), pyrope O-145 (Al, Fe, Mg), fluorapatite (P), orthoclase (K), albite (Na), Ba-Si-glass Gl-10 (Ba), Sr-Si-glass Gl-11 (Sr), V_2O_5 (V). Peak overlaps for $CaK\beta$-$K\alpha$ and $SiK\alpha$-$SrL\alpha$ were compensated automatically by the instrument software, and a matrix correction using the *ZAF* algorithm was applied to raw data prior to recalculation into major oxides. The relative analytical accuracy was within 2% for >5 wt.% elements, and ~5% for ⩽2 wt.% elements (Na, K, Al, Fe, Mg, Ba, Sr, V).
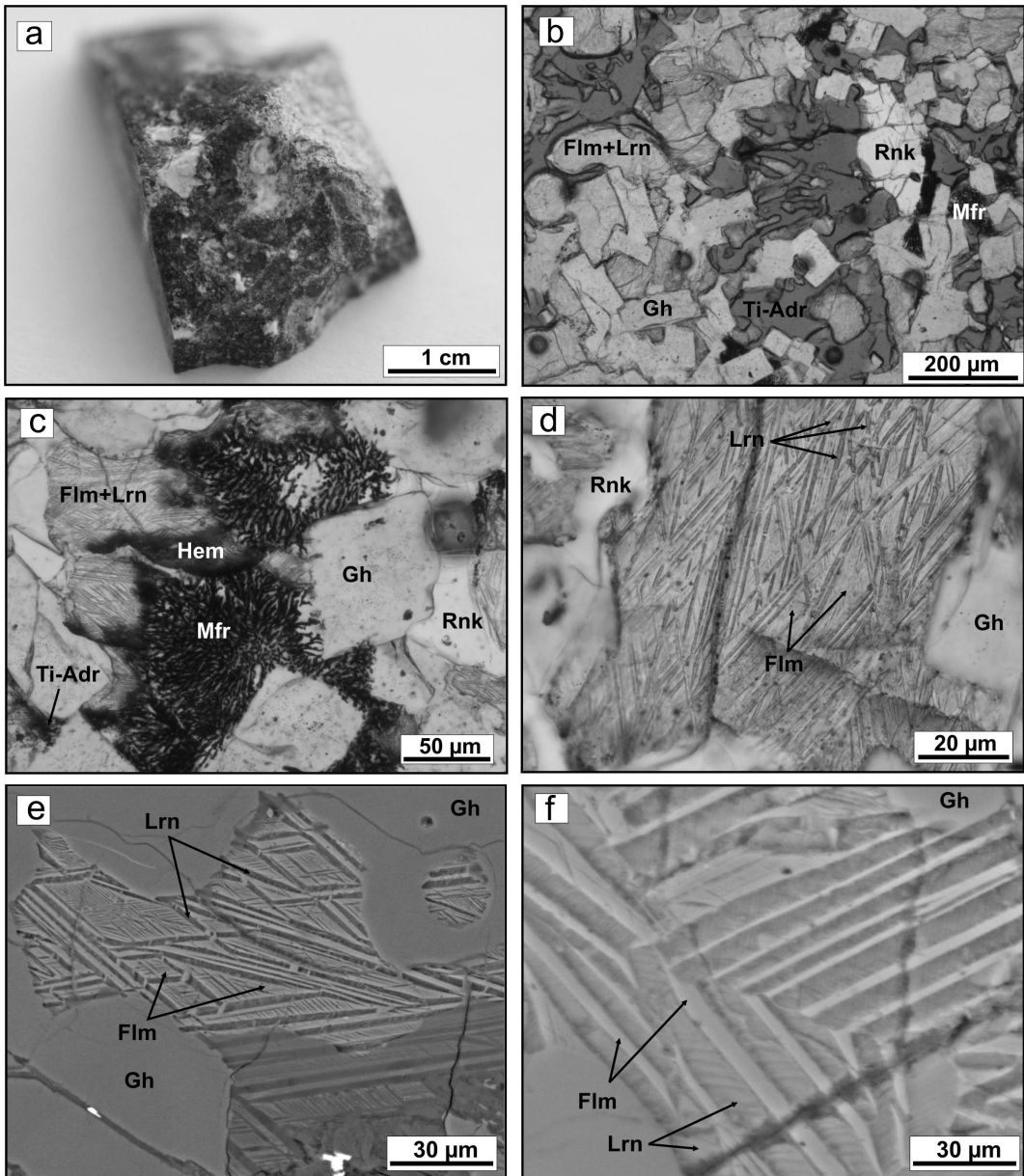
FIG. 1. (*a*) Paralava holotype sample YV-402 with retrograde minerals, namely calcium silicate hydrates and calcite (white) filling vesicles in the melt rock; (*b−f*) morphological diversity of minerals in flamite-bearing paralava; (*b*) a mosaic of squarish gehlenite and anhedral grains of flamite, rankinite and Ti-rich andradite with tubular inclusions of flamite in Ti-rich andradite (plane-polarized light); (*c*) tubular inclusions of magnesioferrite in rankinite, squarish gehlenite crystals and lamellar aggregate of larnite and flamite (plane-polarized light); (*d,e,f*) larnite (β-Ca$_2$SiO$_4$) lamellae in P,Na,K-doped α-Ca$_2$SiO$_4$ matrix; (*d*) plane-polarized light; (*e,f*) BSE images (Gh = gehlenite, Hem = hematite, Mfr = magnesioferrite, Rnk = rankinite, Ti-Adr = Ti-andradite, Flm = flamite, Lrn = larnite [Mineral symbols according to Whitney and Evans (2010)].

TABLE 1. Compositions of minerals associated with flamite (holotype sample YV-402).

Mineral	Larnite	Rankinite	Gehlenite	Perovskite	Magnesio-ferrite	Ti-rich andradite
n	11	12	12	7	5	21
SiO_2	32.25	41.54	24.75	2.28	0.25	23.73
TiO_2	n.a.	0.09	0.09	45.82	0.06	13.48
ZrO_2	n.a.	0.02	n.a.	n.a.	n.a.	0.34
Cr_2O_3	n.a.	b.d.	b.d.	1.78	8.86	1.18
V_2O_5	0.04	n.a.	n.a.	0.05	n.a.	n.a.
Al_2O_3	0.02	b.d.	26.36	0.79	4.28	2.02
Fe_2O_3*			6.95	6.63	59.30	26.78
FeO*	0.02	0.17	0.27		8.07	
MnO	n.a.	n.a.	n.a.	b.d.	0.67	n.a.
MgO	0.07	0.07	1.38	0.03	10.17	0.09
NiO	n.a.	n.a.	n.a.	b.d.	6.39	n.a.
ZnO	n.a.	n.a.	n.a.	b.d.	0.90	n.a.
CaO	63.71	58.04	39.77	41.96	0.60	32.69
SrO	0.14	b.d.	n.a.	n.a.	n.a.	n.a.
Na_2O	0.61	0.04	0.27	n.a.	n.a.	n.a.
K_2O	0.52	b.d.	0.1	n.a.	n.a.	n.a.
P_2O_5	2.35	0.13	b.d.	n.a.	n.a.	0.06
Total	99.73	100.09	99.93	99.33	99.55	100.38
Calculated on:	4O	5 cations	5 cations	2 cations and 3O	3 cations and 4O	8 cations
Si	0.93	1.99	1.16	0.05	0.01	2.05
Ti		0.00	0.00	0.77	0.00	0.88
Zr						0.01
Cr		0.00	0.00	0.03	0.24	0.08
V	0.00			0.00	0.00	
Al	0.00	0.00	1.46	0.02	0.18	0.21
Fe^{3+}			0.24	0.11	1.56	1.74
Fe^{2+}	0.00	0.01	0.01		0.24	
Mn		0.00	0.00	0.00	0.02	0.00
Mg	0.00	0.00	0.10	0.00	0.53	0.01
Ni				0.00	0.18	
Zn				0.00	0.02	
Ca	1.97	2.98	2.00	1.01	0.02	3.02
Na	0.03	0.00	0.02	0.00		0.00
K	0.02	0.00	0.01			0.00
P	0.06	0.01	0.00			

* FeO/Fe_2O_3 calculated on charge balance; b.d.= below detection; n.a. = not analysed; *n* = average of analyses.

Raman spectra were recorded on a Horiba Jobin Yvon LabRAM HR800 spectrometer with a 1024 pixel LN/CCD detector using the 514.5 nm emission line of an Ar^+ ion laser with 50 mW maximum beam power (up to 17 mW on the sample surface). Spectra were collected in back-scattered geometry using an Olympus BX41 microscope (Goryainov *et al.*, 2012, 2014). The resolution of the recorded spectrum was ~2.2 cm^{-1} at a Raman shift of ~3000 cm^{-1}. This resolution was achieved by using a 1800 mm^{-1} grating and equal 150 μm slit and pin hole sizes. The microscope with an Olympus PlanLWD $50\times$ objective lens of working distance 11 mm with a 0.5 numerical aperture provides a focal spot diameter of ~2 μm on the sample surface. The microscope with an Olympus $50\times$ objective lens of working distance = 0.37 mm with 0.75 numerical aperture produces a focal spot diameter of ~2 μm. Raman spectra

were deconvoluted into Voigt amplitude functions using *PeakFit* software (Canberra Industries, 2002).

Single-crystal XRD studies of flamite were carried out using an Oxford Diffraction Xcalibur Gemini diffractometer, Mo$K\alpha$, λ = 0.71073 Å (Novosibirsk State University, Novosibirsk). Diffraction data were collected with ω scans. A total of 151,582 intensities were collected to 55º2θ using 20 s per 1º frames with a crystal-to-detector distance of 8.5 cm. Data were processed using *CrysAlis Pro* (Oxford Diffraction, 2008). A semi-empirical absorption correction was applied using the multi-scan technique. The structure was solved and refined with the *SHELX-97* package (Sheldrick, 2008).

The PXRD data were collected on a Thermo Scientific ARL X'TRA diffractometer equipped with a Peltier cooled Si(Li) solid state detector (Cu$K\alpha$ radiation) at IGM (Novosibirsk). A sintered alumina plate (SRM 1976, a = 4.75885(11), c = 12.993(2) Å) was used as an external standard. The step-scan data collection mode was employed, with steps of 0.02º and 8 s count time for each step. The 2θ range was 5−60º.

Appearance, morphology and physical and optical properties of flamite

Flamite occurs as 100−250 µm anhedral crystals with typical lamellar textures (Fig. 1*b*−*f*) filling interstitial areas between squarish gehlenite crystals (40−100 µm) and as intergrowths with rankinite and Ti-rich andradite. Occasionally there are hematite inclusions at the boundaries between flamite and larnite lamellae. Tubular inclusions of cloudy flamite (up to 50 µm) occur in large poikilitic Ti-rich andradite (0.5−1 mm) and gehlenite (500 µm) crystals. Small inclusions (1−2 µm) of flamite hosted by rankinite coexist with magnesioferrite and fine, devitrified silicate melt inclusions (Fig. 2).

Two types of symmetry-related domain structures of larnite (β-Ca_2SiO_4) are set in a flamite (α-Ca_2SiO_4 (ss)) matrix. The striations intersect at 60º or 120º in cross-sections perpendicular to the c_α axis of the host. In other sections, lamellae intersect at 27º, 54º or 81º, which is consistent with data reported for synthetic analogues of the minerals (Fukuda, 2001). The orientation relationships between the host flamite and the β-Ca_2SiO_4 lamellae are $\{11\bar{2}0\}_\alpha$ ‖ $\{100\}_\beta$ and $<0001>_\alpha$ ‖ $<010>_\beta$, which corresponds to the relative matrix lamellar orientations found by Fukuda and Maki (1989) in synthetic dicalcium silicates. Most larnite lamellae show $\{100\}$ twining. Unlike unaltered flamite, larnite was partly hydrated and converted into calcium silicate hydrates. The extraction of flamite single crystals fit for structure refinement from the fine-grained mineral aggregate was precluded by its intimate intergrowth with larnite.

Flamite is pale yellow or grey (Fig. 1) with a white streak. It is transparent with a vitreous
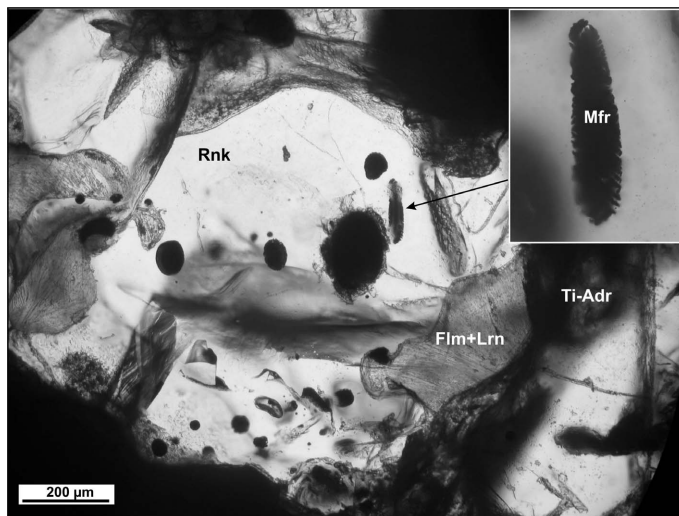
FIG. 2. Ferrite and fine-devitrified silicate melt inclusions in rankinite coexisting with flamite (holotype sample YV-402). Flm = flamite, Lrn = larnite, Mfr = magnesioferrite, Rnk = rankinite, Ti-Adr = Ti-rich andradite.

lustre and does not fluoresce under ultraviolet light. Neither cleavage nor parting was observed. The mineral has a brittle, irregular fracture. The Mohs hardness is $5-5\frac{1}{2}$ and microhardness is $VHN_{50} = 579-753$ kg mm^{-2} (mean 706 kg mm^{-2}). The density calculated from unit-cell dimensions and EMPA data is 3.264 g cm^{-3}. Better physical or optical characterization of the mineral was impossible because of its small grain size and intimate intergrowth with larnite.

Optical properties were measured with a Bloss spindle stage at 589 nm using a gel filter. Flamite is non-pleochroic and uniaxial positive, with refraction indexes $\omega = 1.634$ and $\varepsilon = 1.640$ (both ±0.002); $Z = \varepsilon$.

Chemical tests

Flamite dissolves in 10% HCl with the formation of a SiO$_2$ gel. Various Ca$_2$SiO$_4$ modifications are identified using diverse techniques (Campbell, 1999). The difference between flamite (α-Ca$_2$SiO$_4$) and larnite (β-Ca$_2$SiO$_4$) is indicated by short-term (20 min) etching of polished plates in distilled water + nital (a solution of alcohol and nitric acid, specifically, 1 ml of conc. HNO$_3$ in 99 ml of anhydrous isopropyl alcohol) and in nital + KOH. In both nital and nital + KOH solutions, flamite dissolves and is much less coloured than larnite. Ca$_2$SiO$_4$ samples etched in nital are yellow to brownish while the samples etched in nital + KOH are blue to greyish. Unlike larnite, flamite does not undergo hydration in experiments or the natural environment.

Raman spectroscopy

Raman spectra of flamite show the 106, 125, 170, 188, 199, 260, 294, 396, 430, 439, 500, 520, 538, 575, 589, 666, 714, 850, 863, 885, 952 and 1003 cm^{-1} bands (Fig. 3). Generally, the bands are associated with vibrations of isolated [SiO$_4$] groups (including the internal $\nu_1-\nu_4$ and external R,T modes) and Ca^{2+} cations (translational T modes): (106, 125) T(Ca), (170, 188, 199) T(Ca)+T(SiO$_4$), (260, 294) T(SiO$_4$)+T(Ca), 396 R(SiO$_4$)+T(Ca), (430, 439) ν_2(SiO$_4$), (500, 520, 538, 575, 589, 666, 714) ν_4(SiO$_4$), (850, 863, 885) $\nu_1+\nu_3$(SiO$_4$), (952, 1003) ν_3(SiO$_4$). This interpretation is consistent with published experimental and theoretical (*ab initio* density functional theory) results (Piriou and McMillan, 1983; Chopelas, 1991; McKeown *et al.*, 2010).

Mineral chemistry

Holotype flamite (sample YV-410) has a consistent composition (Table 2) of 58.27 to 61.23 wt.% CaO, 28.14 to 30.17 wt.% SiO$_2$, 6.01 to 8.55 wt.% P$_2$O$_5$, 1.12−1.98 wt.% Na$_2$O and 1.40−2.04 wt.% K$_2$O. Calcium content decreases with increasing P, Na and K (Fig. 4). The empirical formula (mean of 21 analyses) is (Ca$_{1.82}$Na$_{0.09}$K$_{0.06}$ (Mg,Fe,Sr,Ba)$_{0.02}$)$_{\Sigma1.99}$(Si$_{0.82}$P$_{0.18}$)$_{\Sigma1.00}$O$_4$. Minor elements (Al, Mg, Fe, V, Ba, Sr) are insignificant (Table 2). Raman spectroscopy of flamite indicates the absence of [CO$_3$]$^{2-}$ groups, as well as (OH)$^-$ groups and H$_2$O (Fig. 3).

Generally, the sample shows an obvious compositional heterogeneity with both α- and β-Ca$_2$SiO$_4$ modifications being present. Flamite is enriched markedly in P, Na and K relative to coexisting larnite (Tables 1 and 2; Fig. 4). Thus, flamite concentrates most of the P and alkalis among the Ca-Al paralava minerals in the holotype sample.

X-ray diffraction results

Five ~50 μm grains, symmetry-related aggregates of flamite and larnite lamellae, were studied by single-crystal XRD analysis. All the selected grains were composed mainly of flamite with the largest amount of P (Ca$_{1.79}$Na$_{0.06}$K$_{0.06}$ [Si$_{0.80}$P$_{0.20}$O$_4$]). Least-squares refinement of 6649 reflections with $I > 10\sigma(I)$ gave $a = 43.3726(18)$, $c = 6.8270(4)$ Å; $V = 11122.2(9)$ Å^3, $Z = 128$ and $a{:}c = 6.353$. Judging by 788 reflections (*hhl*) with $l = 2n + 1$, flamite lacks c glides and hence has a lower space-group symmetry than the high-temperature α-Ca$_2$SiO$_4$ phase (space group $P6_3/mmc$). The E-value statistics indicate the non-centrosymmetric space group $P6_3$ (no. 173). The unit cell of flamite has a volume 64 times larger than that of high-temperature α-Ca$_2$SiO$_4$ because the a (and hence b) parameters are 8 times larger. Symmetry reduction in flamite may result from ordering of SiO$_4$ and PO$_4$ tetrahedra, as well as atom displacements. The positions of Ca and Si atoms are generally similar to those in the α-Ca$_2$SiO$_4$ and α'-Ca$_2$SiO$_4$ structures. However, larnite present as thin intergrowths with flamite prevents the reliable localization of O positions in the flamite structure. Data for d spacings (in Å for Cu$K\alpha$) are provided in Table 3.
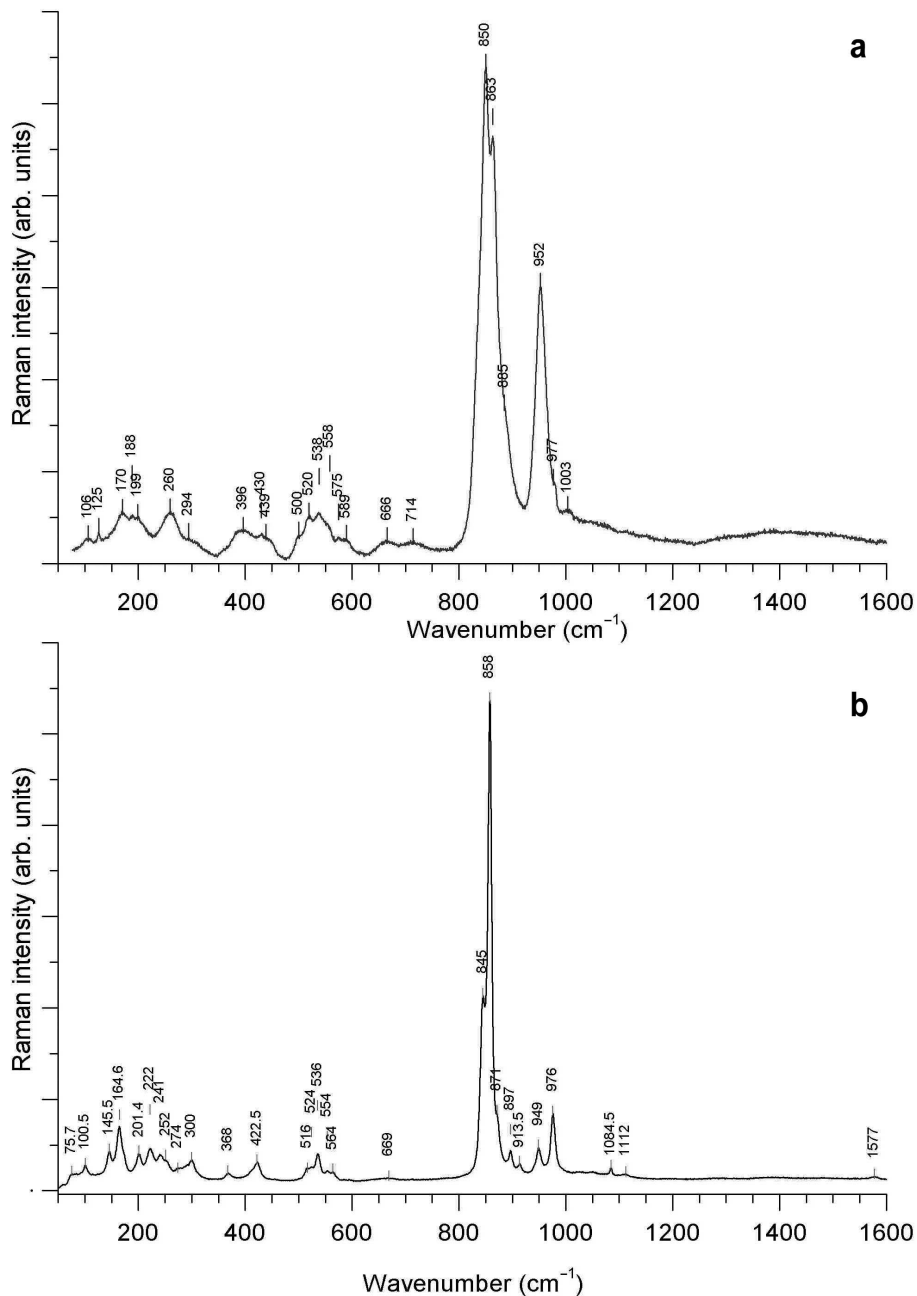
FIG. 3. Raman spectra of flamite (*a*) and larnite (*b*), holotype specimen YV-402.

Relationship to other minerals

Flamite differs from all calcium disilicate modifications known as natural minerals in its chemistry, crystal system, space group, unit-cell parameters, strongest lines in the XRD pattern, optical data, strongest Raman bands and density (Table 4). These properties indicate that flamite is a new mineral. Flamite is a new member of a

TABLE 2. Composition of holotype flamite (sample YV-402).

Sample	1	s.d.	Range	2	3	4	5	6
n	21							
SiO_2	28.87	0.59	28.14−30.17	28.39	28.44	28.35	28.42	29.58
Al_2O_3	0.04	0.02	0−0.08	0.06	0.04	0.04	0.05	0.04
FeO	0.15	0.12	0−0.48	0.08	0.11	0.08	0.05	0.29
MgO	0.16	0.10	0.08−0.55	0.10	0.15	0.12	0.23	0.24
V_2O_5	0.10	0.04	0−0.16	0.12	0.07	0.13	0.09	0.09
BaO	0.05	0.04	0−0.17	0.02	0.02	0.06	0.09	0.08
SrO	0.24	0.05	0.17−0.35	0.32	0.26	0.25	0.25	0.19
P_2O_5	7.38	0.74	6.01−8.55	8.55	8.27	8.08	7.87	6.69
CaO	59.76	0.82	58.27−61.23	59.02	58.27	58.94	58.9	59.85
K_2O	1.73	0.17	1.40−2.04	1.82	2.04	1.86	1.86	1.41
Na_2O	1.55	0.26	1.12−1.98	1.93	1.84	1.71	1.59	1.63
Total	100.03			100.41	99.50	99.62	99.39	100.1
Calculated on: 4O								
Si	0.82			0.80	0.81	0.81	0.81	0.84
Al	0.00			0.00	0.00	0.00	0.00	0.00
Fe	0.00			0.00	0.00	0.00	0.00	0.01
V	0.00			0.00	0.00	0.00	0.00	0.00
Mg	0.01			0.00	0.01	0.01	0.01	0.01
Ca	1.82			1.79	1.78	1.80	1.80	1.82
Ba	0.00			0.00	0.00	0.00	0.00	0.00
Na	0.08			0.11	0.10	0.09	0.09	0.08
K	0.06			0.07	0.07	0.07	0.07	0.06
Sr	0.00			0.01	0.00	0.00	0.00	0.00
P	0.18			0.20	0.20	0.19	0.19	0.16

n : average of analyses; s.d.: standard deviation.

TABLE 3. Experimental PXRD pattern of flamite (Cu$K\alpha$ = 1.54178 Å, Bragg-Brentano geometry, strongest lines in bold).

h	k	l	d (Å)	I
0	8	1	3.875	10
−4	8	2	2.897	19
0	**8**	**2**	**2.765**	**44**
−4	**14**	**1**	**2.759**	**42**
−8	**16**	**0**	**2.713**	**100**
−8	**16**	**1**	**2.518**	**29**
−4	16	1	2.445	13
−2	12	2	2.402	23
0	16	1	2.22	15
−4	16	2	2.077	9
−8	20	1	2.058	10
−4	20	1	1.967	18
0	16	2	1.937	13
0	20	1	1.813	15
−4	**20**	**2**	**1.762**	**32**

group in the sense of Mills *et al.* (2009) of Ca-silicate minerals in which structures are all derived from that of K_2SO_4. This group includes merwinite $(Ca_3Mg(SiO_4)_2)$ and bredigite $(Ca_7Mg(SiO_4)_4)$ as well as larnite.

Dicalcium orthosilicate (Ca_2SiO_4) has at least five polymorphs. The structures of α'_H, α'_L and β-forms are derived from the high-temperature pure α-Ca_2SiO_4 and/or α-Ca_2SiO_4 (ss) by progressive symmetry decrease. The α−α'_H and β-γ phase transitions are reconstructive, while α'_H−α'_L and α'_L−β are displacive (Taylor, 1997; Campbell, 1999; Fukuda, 2001). Both α-Ca_2SiO_4 (ss) and β-Ca_2SiO_4 (ss) can be quenched, which allows the natural occurrence of flamite and larnite (Table 4; Fig. 5).

Calcio-olivine γ-Ca_2SiO_4 (*Pbnm*) is the only Ca_2SiO_4 modification thermodynamically stable under ambient conditions, but the natural analogue is extremely rare. It was found in the Marble Canyon skarns, USA, coexisting with the
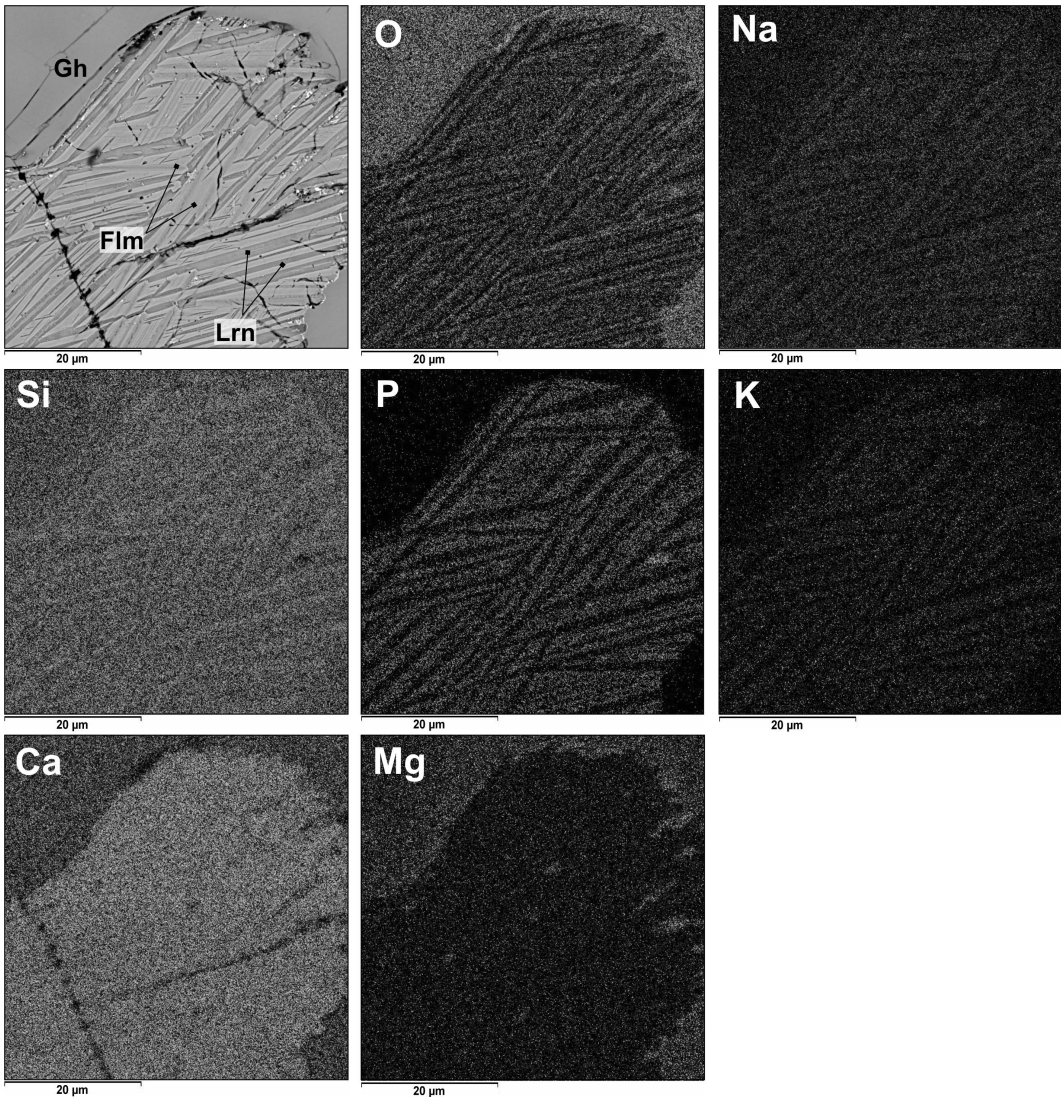
FIG. 4. BSE image and elemental maps for a lamellar aggregate of P, K Na-enriched flamite (Flm) and larnite (Lrn). Gh = gehlenite.

β- and α′-Ca_2SiO_4 forms (Bridge, 1966) (Table 4). A later discovery was in burnt coal spoil heaps of the Kopeisk mining district, Chelyabinsk region, Southern Urals, Russia, and described as "podnoginite" (Chesnokov et al., 1998). However, the mineral has an anthropogenic origin and was not approved as a valid mineral species by the IMA. Rietveld refinement of the calcio-olivine crystal structure was later determined by Gobechiya et al. (2008) in skarn xenoliths from Kabardino-Balkaria, Russia.

The monoclinic β-Ca_2SiO_4 phase ($P2_1/n$) (Table 4) is stable at high pressure and metastable under ambient conditions. However, it is larnite, the natural analogue of this phase doped with small amounts of P, Al, Fe and Na, that is common in high-temperature, low-pressure Ca-rich assemblages in contact metamorphic aureoles and xenoliths (Reverdatto, 1973; Grapes, 2011), as well as Ca-rich pyrometamorphic rocks (Gross, 1977, 1984; Sharygin et al., 2008, 2013; Sokol et al., 2014). The doped β-Ca_2SiO_4 phase does not

591

TABLE 4. Comparative data for flamite, natural and synthetic nagelschmidtite, larnite and calcio-olivine.

	Flamite (α-Ca$_2$SiO$_4$)	Nagelschmidtite natural	Nagelschmidtite synthetic	Larnite (β-Ca$_2$SiO$_4$)	Calcio-olivine (γ-Ca$_2$SiO$_4$)
Formula Crystal system Space group Unit-cell parameters	(Ca,Na,K)$_2$(Si,P)O$_4$ Hexagonal $P6_3$ a = 43.3726(18) Å c = 6.8270(4) Å α = 90° β = 90° γ = 120° V = 11122.2(9) Å^3 Z = 128	α-Ca$_2$SiO$_4$·Ca$_{1.5}$(PO$_4$) Hexagonal (?) not determined not determined	Ca$_7$(SiO$_4$)$_2$(PO$_4$)$_2$ Hexagonal $P6_1$ a = 10.82 Å c = 21.46 Å V = 2176 Å^3 Z = 6	Ca$_2$SiO$_4$ Monoclinic $P2_{1/n}$ a = 5.5051(3) Å b = 6.7551(3) Å c = 9.3108(5) Å β = 94.513(4)° V = 345.17(3) Å^3 Z = 4	Ca$_2$SiO$_4$ Orthorhombic $Pbnm$ a = 5.07389(7) Å b = 11.21128(14) Å c = 6.75340(9) Å V = 384.170(5) Å^3 Z = 4
Strongest reflections of the PXRD: d,Å (I)	2.765(44) 2.759(42) 2.713(100) 2.518(29) 1.762(32)	3.45(m) 2.83(vs) 2.29(w) 1.94(m) 1.84(m, diff.)	3.882(80) 3.456(80) 2.829(100) 2.684(100) 2.209(80) 1.946(80) 1.740(80) 1.525(80) 1.488(80)	2.878(28) 2.793(100) 2.782(98) 2.747(89) 2.732(35) 2.717(35) 2.609(62) 2.282(29) 2.189(55) 1.984(33)	2.730(100) 3.014(90) 2.752(70) 1.909(53) 3.815(35) 4.323(35) 1.636(19)
Optical data	Uniaxial (+) ω = 1.634(2) ε = 1.640(2)	Usually uniaxial (+) rarely biaxial (+) ω = 1.638 ε = 1.652 2V $\approx$ 0°	Uniaxial (+) ω = 1.667 ε = 1.677 2V = low	Biaxial (+) α = 1.700–1.715 β = 1.715–1.723 γ = 1.725–1.740 2V$_{(meas.)}$ = 60–63°	Biaxial n_p = 1.642(2) n_m = 1.652(2) n_g = 1.657(2) 2V$_{(meas)}$ = −69(2)−81(3)°
The strongest Raman bands (cm^{-1})	850 863 952	not determined	not determined	845 858 976	not determined
Density (g cm^{-3})	3.264 (calc.)	not determined	2.998 (calc.)	D_x 3.315	2.98 (calc.)
Reference	This work	Gross (1977); Fleischer *et al.* (1978)	Heller and Taylor (1956); Sugiyama *et al.* (2010)	Deer *et al.* (1986); Mumme *et al.* (1995); Yamnova *et al.* (2011); this work	Gobechiya *et al.* (2008); Zadov *et al.* (2009)
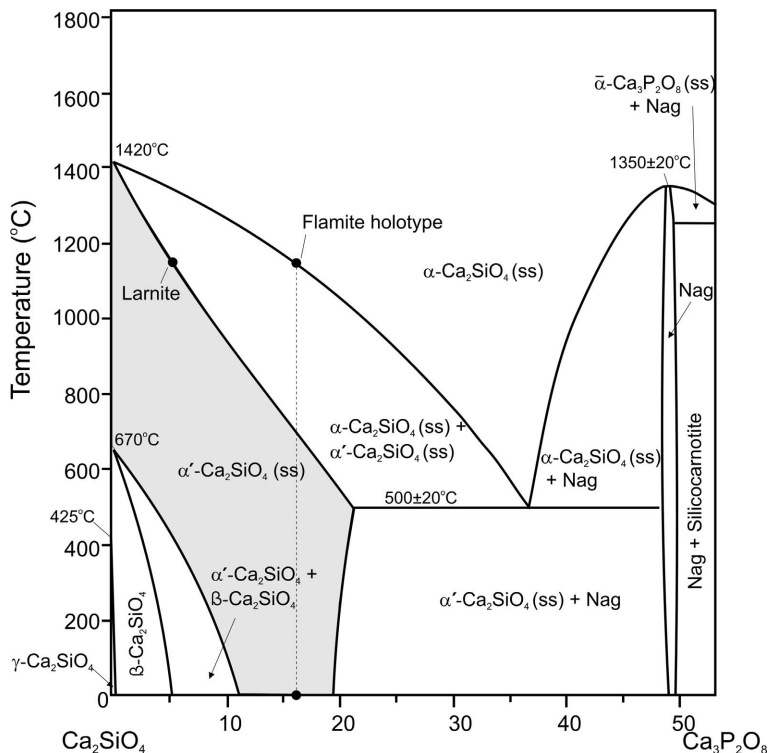
FIG. 5. Flamite (α-Ca_2SiO_4 (ss)) holotype and coexisting larnite compositions projected onto the system Ca_2SiO_4–$Ca_3P_2O_8$. The diagram is modified after Fix *et al.* (1969). Nag = nagelschmidtite.

transform to stable γ-Ca_2SiO_4 on cooling, whereas pure β-Ca_2SiO_4 inverts completely to γ-Ca_2SiO_4 (Taylor, 1997; Campbell, 1999; Fukuda, 2001; Yamnova *et al.*, 2011).

Orthorhombic α'_H-Ca_2SiO_4 (*Pnma*) and α'_L-Ca_2SiO_4 (*Pna2_1*) phases are stable within the temperature interval 680–1160°C (Taylor, 1997). The α'-Ca_2SiO_4 modification has been found in Nature (Bridge, 1966; Gross, 1977). In the latter case (Gross, 1977), the mineral was misidentified as bredigite. The properties of the mineral were determined only partly in both cases, and the compounds have never received the status of a mineral species.

The pure α-Ca_2SiO_4 phase ($T = 1425$–2150°C) is not stable at ambient temperature, and it has never been found in Nature. In the cement industry (clinker production), α-Ca_2SiO_4 is stabilized by the dopants Ba, Sr, P ($\pm$ Na, K), Fe, Al and B, which effectively depress both the transition rate of α-Ca_2SiO_4 (ss)$\rightarrow\alpha'_H\rightarrow\alpha'_L$ and the transformation temperature (Taylor, 1997; Campbell, 1999; Fukuda, 2001). Most of the

doped compositions are liable to quenching and can be preserved under ambient conditions. Flamite can be considered as the natural analogue of α-Ca_2SiO_4 (ss), stabilized by P, Na and K impurities (Fig. 5; Table 4), although as noted above it has an 8*a* superstructure of the high-temperature phase.

Synthetic nagelschmidtite $Ca_7(SiO_4)_2(PO_4)_2$ (*P6_1*) obviously differs from flamite $(Ca,Na,K)_2(Si,P)O_4$ (*P6_3*) in having much more P_2O_5 (19 wt.%), as well as the space group, XRD pattern and optical characteristics; the unit-cell parameters suggest that it has a 3*c* superstructure of high-temperature α-Ca_2SiO_4 (Table 4). Natural nagelschmidtite was first identified in combustion metamorphic rocks of the Hatrurim Basin (Gross, 1977). Gross (1977) characterized the holotype sample as an ultra-thin lamellar aggregate of nagelschmidtite and larnite. Instrumental facilities at that time were insufficient to determine the unit-cell parameters, space group and compositions of individual nagelschmidtite lamellae in the aggregate. Therefore, the IMA approved the new

mineral with an incomplete set of parameters (IMA-1987 s.p., Fleischer *et al.*, 1978), which rules out a full comparison of the mineral. According to Gross (1977), the average bulk P_2O_5 content reaches 8.27 wt.% in the nagelschmidtite-larnite aggregate and nagelschmidtite alone can be expected to contain much more P_2O_5. The presence of nagelschmidtite in the lamellar intergrowth was supported by the optical characteristics of the two phases and by XRD patterns of the analysed material (Gross, 1977). Thus, a review of Gross (1977) data indicates that the mineral identified and described was natural nagelschmidtite rather than a P-, Na- and K-doped analogue of an α-Ca_2SiO_4 phase, such as flamite.

Petrogenesis

Flamite-bearing rock forms by combustion metamorphism at ultrahigh temperatures and ambient pressures as a result of spontaneous ignition of bitumen and gas. This is a new type of melt rock within the Hatrurim Formation (Sharygin *et al.*, 2006; Vapnik *et al.*, 2007; Sokol *et al.*, 2008, 2010; Seryotkin *et al.*, 2012). The local temperatures of fuel combustion were high enough (at least 1400ºC) to cause near-surface total decarbonation and subsequent local melting of Ca-rich parent rocks, namely chalky marine sediments with variable amounts of marl (clay) and phosphorites. The morphology of flamite crystals and the presence of ferrite and fine, devitrified melt inclusions in rankinite provide strong evidence for crystallization from a Ca-rich melt (Figs 1 and 2). Crystallization began with gehlenite, followed by P- and alkali-rich dicalcium silicate [homogeneous α-Ca_2SiO_4 (ss)] and finally by rankinite and Fe-rich minerals, such as Ti-rich andradite, magnesioferrite and hematite.

In terms of crystal chemistry, flamite is the natural analogue of α-Ca_2SiO_4 (ss) stabilized by P, K and Na during paralava quenching. The stabilizing effect of these dopants and the upper temperature limit of quenching (~1280ºC) are known for industrial belite-rich cement clinkers (Fukuda, 2001). The paralava cooling conditions can be reconstructed from symmetry-related lamellar structures of larnite and flamite indicating prolonged heating of an originally homogeneous α-Ca_2SiO_4 (ss) phase at ~1200ºC. As a result, α-Ca_2SiO_4 (ss) decomposed into flamite enriched in P and alkalis and an α'-Ca_2SiO_4 phase depleted in these elements, the two phases being

in equilibrium at ~1200ºC (Fig. 5). By analogy with industrial clinkers, the time of exposure to high temperatures may range from a few hours to a few days (Fukuda, 2001; Campbell, 1999). The cooling rate at *T* <1200ºC was evidently rapid enough to ensure quenching of flamite, while the α'-Ca_2SiO_4 phase became largely inverted to larnite (β-Ca_2SiO_4), and {100} polysynthetic twining formed within the respective lamellae. Details of this process are given by Grove (1983). At the Earth's surface, flamite behaves as an inert phase showing no evidence of hydration, unlike larnite, which was partly converted to calcium silicate hydrates.

References

Bentor, Y.K. and Vroman, A. (1960) *The Geological Map of Israel 1:100000, Sheet 16 – Mount Sedom (with explanatory note)*. Geological Survey of Israel, Jerusalem.

Bridge, T.E. (1966) Bredigite, larnite and γ-dicalcium silicates from Marble Canyon. *American Mineralogist*, **51**, 1766–1774.

Britvin, S.N., Vapnik, Y., Polekhovsky, Y.S. and Krivovichev, S.V. (2013) Murashkoite, IMA 2012-071. CNMNC Newsletter No. 15, February 2013, page 8; *Mineralogical Magazine*, **77**, 1–12.

Britvin, S.N., Murashko, M., Vapnik, Y., Polekhovsky, Y.S. and Krivovichev, S.V. (2014*a*) Negevite, IMA 2013-104. CNMNC Newsletter No. 19, February 2014, page 166; *Mineralogical Magazine*, **78**, 165–170.

Britvin, S.N., Murashko, M., Vapnik, Y., Polekhovsky, Y.S. and Krivovichev, S.V. (2014*b*) Halamishite, IMA 2013-105. CNMNC Newsletter No. 19, February 2014, page 167; *Mineralogical Magazine*, **78**, 165–170.

Britvin, S.N., Murashko, M., Vapnik, Y., Polekhovsky, Y.S. and Krivovichev, S.V. (2014*c*) Zuktamrurite,

IMA 2013-107. CNMNC Newsletter No. 19, February 2014, page 167; *Mineralogical Magazine*, **78**, 165−170.

Burg, A., Starinsky, A., Bartov, Y. and Kolodny, Y. (1992) Geology of the Hatrurim Formation ("Mottled Zone") in the Hatrurim basin. *Israel Journal of Earth Sciences*, **40**, 107−124.

Campbell, D.H. (1999) *Microscopical Examination and Interpretation of Portland Cement and Clinker. 2nd edition*. Portland Cement Association, Skokie, Illinois, USA.

Canberra Industries Inc (2002) *Model S506 Interactive Peak Fit, User's Manual*. Canberra Industries Inc, Canberra.

Chesnokov, B., Kotrly, M. and Nisanbajev, T. (1998) Brennende Abraumhalden und Aufschlüsse im Tscheljabinsker Kohlenbecken − eine reiche Mineralienküche. *Mineralien-Welt*, **9(3)**, 54−63.

Chopelas, A. (1991) Single crystal Raman spectra of forsterite, fayalite and monticellite. *American Mineralogist*, **76**, 1101−1109.

Deer, W.A., Howie, R.A. and Zussman, J. (1986) *Rock-Forming Minerals*. 2nd edition. Longmans, London and New York, pp. 248−255.

Fix, W., Heymann, H. and Heinke, R. (1969) Subsolidus relations in the system $2CaO \cdot SiO_2 - 3CaO \cdot P_2O_5$. *Journal of the American Ceramic Society − Discussion and Notes*, **52**, 346−347.

Fleuscher, M., Cabri, L.J. Chao, G.Y. and Pabst, A. (1978) New mineral names. *American Mineralogist*, **63**, 424−427.

Fukuda, K. (2001) Recent progress in crystal chemistry of belite: intracrystalline microtextures induced by phase transformations and application of remelting reaction to improvement of hydration reactivity. *Journal of the Ceramic Society of Japan*, **109**, 43−48.

Fukuda, K. and Maki, I. (1989) Orientation of β-Ca_2SiO_4 solid solution lamellae formed in the host α-phase. *Cement and Concrete Research*, **19**, 913−918.

Heller, L. and Taylor, H.F.W. (1956) *Crystallographic Data for the Calcium Silicates*. HMSO, London.

Galuskin, E.V., Galuskina, I.O., Pakhomova, A., Armbruster, T., Vapnik, Y., Dzierżanowski, P. and Murashko, M. (2013a) Aradite, IMA 2013-047. CNMNC Newsletter No. 17, October 2013, p. 3001; *Mineralogical Magazine*, **77**, 2997−3005.

Galuskin, E.V., Gfeller, F., Armbruster, T., Sharygin, V.V., Galuskina, I.O., Krivovichev, S.V., Vapnik, Y., Murashko, M., Dzierżanowski, P. and Wirth, R. (2013b) Fluorkyuygenite, IMA 2013-043. CNMNC Newsletter No. 17, October 2013, page 3000; *Mineralogical Magazine*, **77**, 2997−3005.

Galuskin, E.V., Gfeller, F., Galuskina, I.O., Armbruster, T., Vapnik, Y., Włodyka, R., Dzierżanowski, P. and

Murashko, M. (2013c) Zadovite, IMA 2013-031. CNMNC Newsletter No. 16, August 2013, page 2708; *Mineralogical Magazine*, **77**, 2695−2709.

Galuskin, E.V., Kusz, J., Gfeller, F., Galuskina, I.O., Vapnik, Y., Dulski, M. and Dzierżanowski, P. (2014) Silicocarnotite, IMA 2013-139. CNMNC Newsletter No. 20, June 2014, p. 553; *Mineralogical Magazine*, **78**, 549−558.

Galuskina, I.O., Vapnik, Y., Prusik, K., Dzierżanowski, P., Murashko, M. and Galuskin, E.V. (2013) Gurimite, IMA 2013-032. CNMNC Newsletter No. 16, August 2013, page 2708; *Mineralogical Magazine*, **77**, 2695−2709.

Goryainov, S.V., Krylov, A.S., Pan, Y., Madyukov, I.A., Smirnov, M.B. and Vtyurin, A.N. (2012) Raman investigation of hydrostatic and nonhydrostatic compressions of OH- and F-apophyllites up to 8 GPa. *Journal of Raman Spectroscopy*, **43**, 439−447.

Goryainov, S.V., Likhacheva, A.Y., Rashchenko, S.V., Shubin, A.S., Afanasiev, V.P. and Pokhilenko, N.P. (2014) Raman identification of lonsdaleite in Popigai impactites. *Journal of Raman Spectroscopy*, **45**, 305−313.

Grapes, R. (2011) *Pyrometamorphism*. 2nd edition. Springer, Berlin.

Gross, S. (1977) The mineralogy of the Hatrurim Formation, Israel. *Geological Survey of Israel Bulletin*, **70**.

Gross, S. (1980) Bentorite. A new mineral from the Hatrurim Area, west of the Dead Sea, Israel. *Israel Journal of Earth Sciences*, **29**, 81−84.

Gross, S. (1984) Occurrence of ye'elimite and ellestadite in an unusual cobble from the "pseudo-conglomerate" of the Hatrurim Basin, Israel. *Geological Survey of Israel, Current Research 1983−84*, 1−4.

Gross, S. and Heller, L. (1963) A natural occurrence of bayerite. *Mineralogical Magazine*, **32**, 723−724.

Gobechiya, E.R., Yamnova, N.A., Zadov, A.E. and Gazeev, V.M. (2008) Calcio-olivine γ-Ca_2SiO_4: I. Rietveld refinement of the crystal structure. *Crystallography Reports*, **53**, 404−408.

McKeown, D.A., Bell, M.I. and Caracas, R. (2010) Theoretical determination of the Raman spectra of single-crystal forsterite (Mg_2SiO_4). *American Mineralogist*, **95**, 980−986.

Mills, S.J., Hatert, F., Nickel, E.H. and Ferraris, G. (2009) The standardisation of mineral group hierarchies: application to recent nomenclature proposals. *European Journal of Mineralogy*, **21**, 1073−1080.

Mumme, W.G., Hill, R.J., Bushnell, Wye G. and Segnit, E.R. (1995) Rietveld crystal structure refinements, crystal chemistry and calculated powder diffraction data for the polymorphs of dicalcium silicate and related phases. *Neues Jahrbuch für Mineralogie, Abhandlungen*, **169**, 35−68.

Murashko, M.N., Chukanov, N.V., Mukhanova, A.A., Vapnik, E., Britvin, S.N., Krivovichev, S.V., Polekhovsky, Y.S. and Ivakin, Yu.D. (2011) Barioferrite $BaFe_{12}^{+3}O_{19}$ a new magnetoplumbite-group mineral from Hatrurim Formation, Israel. *Geology of Ore Deposits*, **53**, 558−563.

Oxford Diffraction (2008) *CrysAlis RED (ver. 1.171.35.15)*. Oxford Diffraction, Abingdon, Oxfordshire, England.

Piriou, B. and McMillan, P. (1983) The high-frequency vibrational spectra of vitreous and crystalline orthosilicates. *American Mineralogist*, **68**, 426−443.

Reverdatto, V.V. (1973) *The Facies of Contact Metamorphism*. Australian National University, Canberra.

Seryotkin, Y.V., Sokol, E.V. and Kokh, S.N. (2012) Natural pseudowollastonite: crystal structure, associated minerals, and geological context. *Lithos*, **133−135**, 75−90.

Sharygin, V.V., Vapnik, Y., Sokol, E.V., Kamenetsky, V.S. and Shagam, R. (2006) Melt inclusions in minerals of schorlomite-rich veins of the Hatrurim Basin, Israel: composition and homogenization temperatures. *ACROFI I Program with Abstracts, 2006*, pp. 189−192.

Sharygin, V.V., Sokol, E.V. and Vapnik, Y. (2008) Minerals of the pseudobinary perovskite-brownmillerite series from combustion metamorphic larnite rocks of the Hatrurim Formation (Israel). *Russian Geology and Geophysics*, **49**, 709−726.

Sharygin, V.V., Lazic, B., Armbruster, T.M., Murashko, M.N., Wirth, R., Galuskina, I.O., Galuskin, E.V., Vapnik, Y., Britvin, S.N. and Logvinova, A.M. (2013) Shulamitite $Ca_3TiFe^{3+}AlO_8$ − a new perovskite-related mineral from Hatrurim Basin, Israel. *European Journal of Mineralogy*, **25**, 97−111.

Sheldrick, G.M. (2008) A short history of SHELX. *Acta Crystallographica*, **A64**, 112−122.

Sokol, E.V., Novikov, I.S., Zateeva, S.N., Sharygin, V.V. and Vapnik, Y. (2008) Pyrometamorphic rocks of the spurrite-merwinite facies as indicators of hydrocarbon discharge zones (the Hatrurim Formation, Israel). *Doklady Earth Sciences*, **420**, 608−614.

Sokol, E., Novikov, I., Zateeva, S., Vapnik, Y., Shagam, R. and Kozmenko, O. (2010) Combustion metamorphic rocks as indicators of fossil mud volcanism: new implications for the origin of the Mottled Zone, Dead Sea rift area. *Basin Research*, **22**, 414−438.

Sokol, E.V., Kokh, S.N., Vapnik, Y., Thiéry, V. and Korzhova, S. (2014) Natural analogues of belite sulfoaluminate cement clinkers from Negev desert, Israel. *American Mineralogist*, **99**, 1471−1487.

Sugiyama, K., Kato, Y. and Mikouch, T. (2010) Structure of nagelschmidtite $Ca_7Si_2P_2O_{16}$. *CD of Abstracts, 20th General Meeting of the IMA, Budapest*, pp. 725.

Taylor, H.F.W. (1997) *Cement Chemistry*, 2nd edition. Tomas Telford Services, London.

Vapnik, Y., Sharygin, V.V., Sokol, E.V. and Shagam, R. (2007) Paralavas in a combustion metamorphic complex: Hatrurim Basin, Israel. *Reviews in Engineering Geology*, **18**, 1−21.

Weber, D. and Bischoff, A. (1994) Grossite ($CaAl_4O_7$) − a rare phase in terrestial rocks and meteorites. *European Journal of Mineralogy*, **6**, 591−594.

Whitney, D.L. and Evans, B.W. (2010) Abbreviations for names of rock-forming minerals. *American Mineralogist*, **95**, 185−187.

Yamnova, N.A., Zubkova, N.V., Eremin, N.N., Zadov, A.E. and Gazeev, V.M. (2011) Crystal structure of larnite β-Ca_2SiO_4 and specific features of polymorphic transitions in dicalcium orthosilicate. *Crystallography Reports*, **56**, 210−220.

Zadov, A.E., Gazeev, V.M., Pertsev, N.N., Gurbanov, A.G., Gobechiya, E.R., Yamnova, N.A. and Chukanov, N.V. (2009) Calcioolivine, gamma-Ca_2SiO_4, an old and New Mineral species. *Geology of Ore Deposits*, **51**, 741−749.